Photoassisted transport in silicon dangling bond wires

Andrii Kleshchonok, Rafael Gutierrez, Christian Joachim, Gianaurelio Cuniberti

Photoassisted transport in silicon dangling bond wires

Andrii Kleshchonok, Rafael Gutierrez, Christian Joachim, and Gianaurelio Cuniberti

Citation: Appl. Phys. Lett. **107**, 203109 (2015); doi: 10.1063/1.4936182
View online: https://doi.org/10.1063/1.4936182
View Table of Contents: http://aip.scitation.org/toc/apl/107/20
Published by the American Institute of Physics

Photoassisted transport in silicon dangling bond wires

Andrii Kleshchonok,[1] Rafael Gutierrez,[1] Christian Joachim,[2,3] and Gianaurelio Cuniberti[1,4,5]
[1]*Institute for Materials Science, Dresden University of Technology, TU Dresden, 01062 Dresden, Germany*
[2]*GNS & MANA Satellite, CEMES-CNRS, 29 Rue J. Marvig, 31055 Toulouse Cedex, France*
[3]*International Centre for Materials Nanoarchitectonics (MANA), National Institute for Materials Science, 1-1, Namiki, Tsukuba, Ibaraki 305-0044, Japan*
[4]*Dresden Center for Computational Materials Science, TU Dresden, 01062 Dresden, Germany*
[5]*Center for Advancing Electronics Dresden, TU Dresden, 01062 Dresden, Germany*

(Received 31 August 2015; accepted 6 November 2015; published online 18 November 2015)

We theoretically investigate charge transport through dangling bond (DB) nanostructures built on a passivated silicon (100) surface by selectively removing hydrogen atoms. We focus on dangling bond wires and on T-junctions. In the latter case, destructive quantum interference effects lead to a strong suppression of charge transport mediated by the DB electronic states. We demonstrate, however, that by applying a time periodic voltage, mimicking irradiation with monochromatic light, a dramatic enhancement of the current up to the μA range can be achieved. This result is however limited by the restriction on the AC field strength and frequency that bulk states should minimally contribute to charge transport; otherwise current leakage will set in. Despite this constraint, transconductance values of the order of 10^{-6} A/V can be achieved, illustrating the potential of the discussed systems to find applications in nanoscale electronics. © *2015 AIP Publishing LLC*.
[http://dx.doi.org/10.1063/1.4936182]

Increasingly faster developments in semiconductor nanotechnologies are allowing to engineer electronic circuits with a lateral precision of few nanometers. However, these conventional "top-down" design strategies are now facing fundamental limitations such as power dissipation and intra-device tunnelling leakage currents. A variety of approaches based on bottom-up engineering have been proposed to overcome these difficulties, involving nanoscale functional objects such as individual carbon nanotubes, molecular systems,[1] silicon nanowires,[2] among others. Nevertheless, despite enormous progress in fabrication technologies as well as in the basic experimental and theoretical understanding of charge transport in nanoscale devices, still many challenges need to be faced, such as scaling problems[3] and low transconductance values of the active devices.[4] Dangling bond (DB) states—built by selectively removing hydrogen atoms from a Si(100)-H (2×1) surface by means of a scanning tunnelling microscope[5]—have attracted considerable interest due to their potential application in the design of planar atomic-scale devices embedded in a silicon matrix.[6–12] DB nanowires can be fabricated with different surface orientations–along and perpendicularly to the Si dimer rows on the (2×1) reconstructed surface. Meanwhile, a mesoscale single-atom transistor,[13] atomic scale interconnects,[14–18] as well as Boolean logic gates[17,19,20] based on DB states have been proposed. Creating a dangling bond on the Si atom introduces localized electronic states in the bulk band gap,[21] resulting in the DB wires being metallic in the ideal case of infinite wires with no surface relaxation.[7] However, in a finite DB wire, due to Jahn-Teller distortions leading to buckling of the Si surface atoms, the metallic character is suppressed and the charge transport response is strongly modified.[14,18,21,22] As a result, the current supported by the DB states can be reduced from μA to few nA at applied bias of the order of 1 V,[7,18,23] which is not suitable for electronic applications. Here, there is a limit to the maximum possible bias voltage: the bias window should not cover the semiconductor conduction and valence bands to prevent the current to leak into the silicon bulk, ensuring in this way that charge transport is mediated only by DB states. In order to overcome these limitations, we propose to use photoassisted transport (PAT) through DB wires that results in a considerable enhancement of electronic current while keeping the DC component fixed at a low bias voltage. Experimentally, PAT is realized by laser irradiation of semiconductor nanostructures[24–27] or by irradiating metallic nanocontacts.[28] Theoretically, a variety of methods have been used such as Floquet theory,[27,29] master equation approaches,[29] scattering matrix methods,[29] and Green's function techniques.[30,31] In this letter, we study two DB structures: (i) a wire built perpendicularly to the surface dimer rows, Fig. 1(a), and (ii) a T-junction wire, Fig. 1(b). The latter has been shown to display pronounced quantum interference mediated suppression of charge transport,[20] and thus offers a good playground to address the influence of PAT in a low conducting system. These DB structures are coupled with two Au nanoelectrodes, see Figs. 1(a) and 1(b), that could be, e.g., UHV transfer printed on the Si surface.[15,16,32] Due to the large number of atoms, our structures were first relaxed with a Density-Functional parametrized Tight-Binding (DFTB) code[38,39] using a conjugate-gradient method with an accuracy up to 10^{-7} eV/Å. The relaxed systems were then used as input for single-point electronic structure calculations at the full DFT level[40] to get the Hamiltonian and Overlap electronic matrices required for the transport calculations. We use the PBE pseudopotential[41] and a double-ζ basis set for Si and triple-ζ for Au. The semiconductor surface was modelled using 8 layers of Si atoms under periodic boundary conditions.

The transport properties were computed using the Landauer formalism[30] combined with Green's function

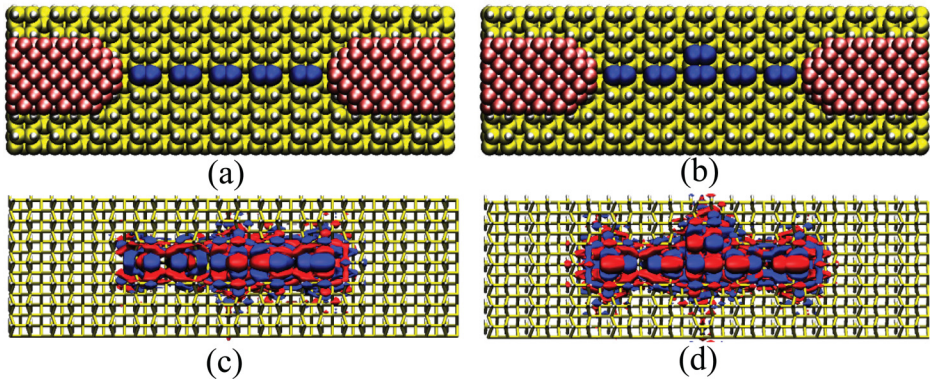

FIG. 1. (a) A wire with dangling bonds (blue) built perpendicularly to the Si dimer rows and (b) a T-junction with 2 additional DBs in parallel. Both wires are contacted at their ends by Au electrodes. In panels (c) and (d) the real part of the electronic wave function of both wires is displayed, showing the spatial distribution of the localized states introduced by the DB in the Si band gap. The asymmetry of the wave function relates to the buckling of the DB atoms.

techniques. The energy dependent quantum mechanical transmission function T_E between left (L) and right (R) gold contacts is calculated as $T_E = Tr(\Gamma_E^L G_E^r \Gamma_E^R G_E^a)$. Here, $G^{r(a)}$ are retarded (advanced) Green's function of the system, describing the DB system and taking into account the coupling to the electrodes by means of self-energy functions $\Sigma^{r(a),L(R)}$. The spectral densities $\Gamma^{L(R)} = i(\Sigma^{r,L(R)} - \Sigma^{a,L(R)})$ encode both the electronic structure of the electrodes surface and the coupling between atoms on the electrodes and on the DB wire. The self-energies are calculated for each electrode using the Lopez-Sancho procedure.[42] The two-terminal current is obtained as $I(V_{dc}) = (2e/h)\int T_E[f_E^{\mathrm{L}} - f_E^{\mathrm{R}}]dE$, with $f_E^{\mathrm{L(R)}}$ being the Fermi function of the left(right) electrode.

The analysis of the electronic structure shows localized π and π^* DB orbitals, see Figs. 1(c) and 1(d), which are mainly derived from Si p_z atomic states.[20] The Fermi energy E_F for both, the wire and the T-junction, lies in the gap between the π and π^* states, as shown in Figs. 2(a) and 2(c), where the corresponding projected density of the states (PDOS) on the Si atoms is plotted. The number of peaks in the transmission function, Fig. 2(b), correlates with the number of DB pairs, and the transmission would reach the unitary limit for an infinite DB wire. If two additional DBs are added to build a T-junction, the transmission around the π and π^* bands is suppressed due to destructive interference. This manifests in the I–V curves (see inset in Fig. 2(a)), leading to a difference of roughly 3 orders of magnitude in the currents through the two DB conformations. The bias window V_{dc}, which allows for DB-mediated charge transport without current leakage into the substrate, is highlighted in grey in Figs. 2(b) and 2(d). Next, we address PAT in both DB nanostructures within the Tien-Gordon (TG) approach[33] combined with Green's function techniques.[30,31] TG-based approaches have proved efficient for gaining an understanding of light-matter interactions in semiconductor nanostructures,[27,34] mesoscopic systems,[35] and in nanojunctions.[30,36,37] We further assume that the potential is dropped only on the electrodes and consider the wide-band limit, which is equivalent to replacing the complex, energy-dependent electrode self-energies by an imaginary constant, which only induces a broadening of the electronic states. This approximation is valid for Au electrodes, where the density of states near the Fermi energy is mostly derived from valence 6s states and is roughly constant. We consider, besides the constant applied voltage V_{dc}, a harmonic driving with amplitude V_{ac}: $V(t) = V_{dc} + V_{ac}\sin(\omega t)$. The experimentally relevant quantities, the linear ($V_{dc} \to 0$) photoconductance G, and the DC-component of the electrical current I are given by[31]

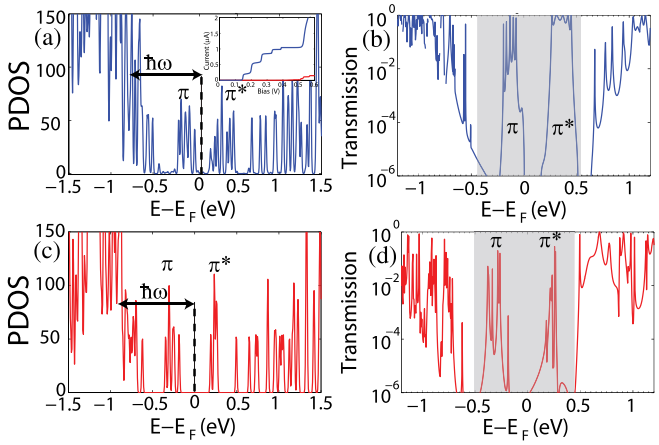

FIG. 2. Projected density of states (PDOS) for the case of (a) wire and (c) T-junction, showing that π and π^* DB states emerge in the Si(100)-H surface band gap. The valence band states become exited by the AC field, when $\hbar\omega$ reaches the Si valence band edge. Panels (b) and (d) show the transmission function of the wire and the T-junction, respectively. The shaded areas indicate the voltage range where the current will be mostly carried by DB states. The inset of panel (a) shows the I–V curves for the wire (blue) and the T-junction (red). Destructive interference effects in the T-junction (see panel (d)) lead to a dramatic current suppression.

$$G_{E_F}(\omega) = \frac{2e^2}{h}\sum_{l=-\infty}^{l=+\infty} |g_l|^2 T_{E_F+l\hbar\omega}, \tag{1}$$

$$I(V,\omega) = \frac{2e^2}{h}\sum_{l=-\infty}^{l=+\infty} |g_l|^2 \int_{-\infty}^{\infty} T_{E+l\hbar\omega}\left[f_E^{\mathrm{L}} - f_E^{\mathrm{R}}\right] dE. \tag{2}$$

Here, $\alpha = eV_{ac}/\hbar\omega$ is a dimensionless parameter, $g_l = J_l\left(\frac{\alpha}{2}\right)$, and J_l is a Bessel function of the first kind of order l. Eqs. (1) and (2) describe inelastic photon-assisted tunnelling processes, where the junction emits or absorbs l photons with energy $\hbar\omega$ (photon sidebands). The photoconductance at the Fermi energy as a function of eV_{ac} and $\hbar\omega$ is shown in Figs. 3(a) and 3(c). For $eV_{ac} < 1$ eV, regions of high and low conductance can be seen when varying the photon energy; they sensitively depend on the position of the sidebands with respect to E_F (either a satellite lies at E_F or their tails provide enough spectral weight at E_F to increase tunnelling). If the AC field strength increases, $eV_{ac} > 1$ eV, while keeping the photon energy roughly below 0.3–0.4 eV, the conductance at E_F is very small as a result of the argument of the Bessel function,

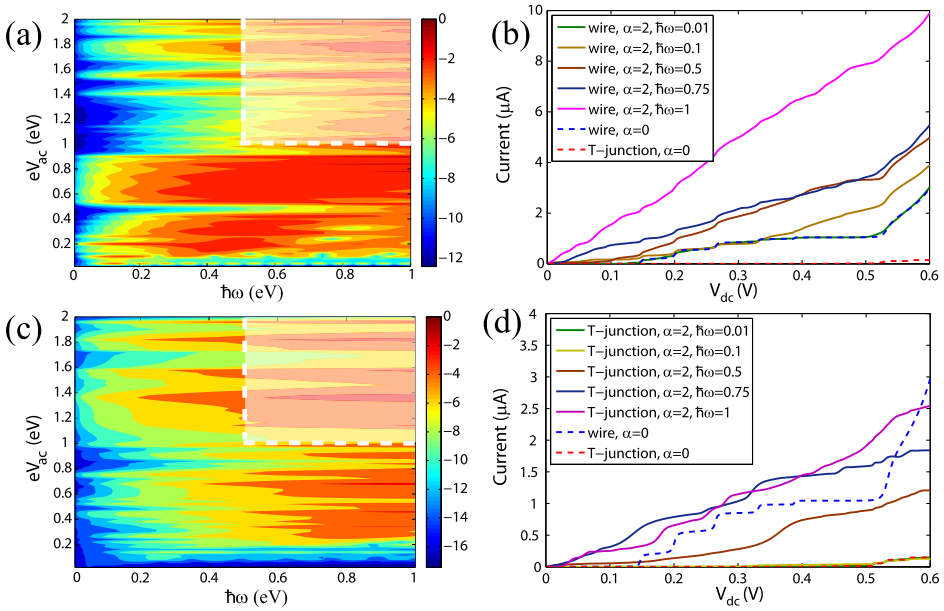

FIG. 3. Photoconductance (1) in logarithmic scale as a function of eV_{ac} and the AC field frequency $\hbar\omega$ for the (a) wire and (c) T-junction geometry. Panels (b) and (d) show the electrical current as a function of the applied DC voltage V_{dc} at various frequencies $\hbar\omega = 0.01, 0.1, 0.5, 0.75, 1\,\text{eV}$ and for $\alpha = 2$. The current of the wire (blue dotted line) and the T-junction (red dotted line) for $\alpha = 0$ are also shown for reference. The shaded area approximately indicates the parameter range, where the current may be partially carried by bulk states.

α, becoming (much) larger than 1. Thus, the weight of $J_l(\alpha)$ goes down with increasing l. Considering that the $l = 0$ contribution at E_F is almost negligible, the first non-vanishing term would be for $l = 1$; if the first satellite is however far from E_F (small $\hbar\omega$), then the conductance is suppressed. If both eV_{ac} and $\hbar\omega$ are large (shaded areas in Figs. 3(a) and 3(c)), states from the bulk bands can be photoexcited and current leakage may eventually set in. As shown in Figs. 3(b) and 3(d), strong current enhancement can be induced when photon sidebands enter the V_{dc} bias window. Notice, however, that V_{dc} needs to be small enough to avoid current leakage into the Si substrate. The low current found in the T-junction (red dotted line in Fig. 3(d)) may be tuned with the help of light irradiation and the resulting current can become even larger than the one of the linear wires, see the blue dotted line in Fig. 3(d), reaching values of few μA. This is due to the fact that photoexcited electrons ($l \neq 0$) do not match the destructive interference conditions of the $l = 0$ ones. The attainable photoassisted current values in the μA range clearly suggest a more favorable application potential for nanoscale devices as when only a DC bias is applied. The fact that an applied AC voltage allows for such a dramatic increase of the current in the case of the T-junction, where the DC current is almost suppressed by destructive interference, suggests that T-junctions might be used as an atomic-scale transistor. Here, a key parameter is the device transconductance, which we defined as the response to the AC drive at fixed DC voltage: $(dI/dV_{ac})|_{V_{dc}=const}$. The current as a function of V_{ac} is shown in Fig. 4. In the case of the T-junction, transconductance values of $(2-3)\cdot 10^{-6}$ A/V are obtained, which are much higher than the response to a top gate voltage in a similar setup,[23] and reach values similar to those reported for a C_{60} molecular transistor.[4] In the case of the linear wire, there is current enhancement under photo-irradiation as well, it displays however a non-monotonic behaviour with V_{ac} (Fig. 4(a)) and the transconductance is lower.

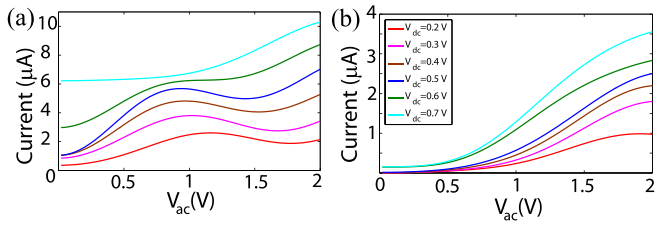

FIG. 4. Current through (a) the DB wire and (b) the T-junction, as a function of AC voltage at AC frequency $\hbar\omega = 0.2\,\text{eV}$, and for $V_{dc} = 0.2, 0.4, 0.6, 0.7\,\text{V}$. The transconductance is computed from these data as dI/dV_{ac}.

In summary, we have investigated charge transport signatures of two atomic-scale dangling bond systems: one made with a linear DB wire and a second built by adding two DB sites to form a T-junction. In the latter case, the current is strongly suppressed due to destructive quantum interference. However, we have shown that interference effects can be counteracted and fine tuned by an applied time-dependent AC field. In particular, photoassisted transport may lead to high transconductance values of $(2-3)\cdot 10^{-6}$ A/V, comparable with the values for a C_{60} single molecule-based transistor. The photoassisted current can be significantly increased and reach up to 10 μA, which we can expect to be of major relevance for potential technological applications.

We thank M. Moskalets for very useful discussions. This work has been funded by the EU within the Project *Planar Atomic and Molecular Scale devices* (PAMS, Project No. 610446). It has also been partly supported by the German Research Foundation (DFG) within the Cluster of Excellence "Center for Advancing Electronics Dresden." Computational resources were provided by the ZIH at TU Dresden.

[1]N. Lorente and C. Joachim, *Architecture and Design of Molecule Logic Gates and Atom Circuits* (Springer-Verlag, Berlin, Heidelberg, 2013).
[2]Y. Huang, X. Duan, Y. Cui, L. J. Lauhon, K.-H. Kim, and C. M. Lieber, Science **294**, 1313 (2001).
[3]N. Collaert, *CMOS Nanoelectronics: Innovative Devices, Architectures, and Applications* (CRC Press, 2012).
[4]C. Joachim, J. Gimzewski, and A. Aviram, Nature **408**, 541 (2000).
[5]S. R. Schofield, P. Studer, C. F. Hirjibehedin, N. J. Curson, G. Aeppli, and D. R. Bowler, Nat. Commun. **4**, 1649 (2013).
[6]M. Y. Simmons, Nat. Phys. **4**, 165 (2008).
[7]M. Kepenekian, R. Robles, C. Joachim, and N. Lorente, Nano Lett. **13**, 1192 (2013).

[8]B. Naydenov and J. J. Boland, Nanotechnology **24**, 275202 (2013).
[9]M. B. Haider, J. L. Pitters, G. A. DiLabio, L. Livadaru, J. Y. Mutus, and R. A. Wolkow, Phys. Rev. Lett. **102**, 046805 (2009).
[10]L. Soukiassian, A. J. Mayne, M. Carbone, and G. Dujardin, Surf. Sci. **528**, 121 (2003).
[11]M. Kolmer, S. Godlewski, R. Zuzak, M. Wojtaszek, C. Rauer, A. Thuaire, J.-M. Hartmann, H. Moriceau, C. Joachim, and M. Szymonski, Appl. Surf. Sci. **288**, 83 (2014).
[12]M. Kolmer, R. Zuzak, G. Dridi, S. Godlewski, C. Joachim, and M. Szymonski, Nanoscale **7**, 12325 (2015).
[13]M. Fuechsle, J. A. Miwa, S. Mahapatra, H. Ryu, S. Lee, O. Warschkow, L. C. L. Hollenberg, G. Klimeck, and M. Y. Simmons, Nat. Nanotechnol. **7**, 242 (2012).
[14]D. R. Bowler, J. Phys.: Condens. Matter **16**, R721 (2004).
[15]P. Doumergue, L. Pizzagalli, C. Joachim, A. Altibelli, and A. Baratoff, Phys. Rev. B **59**, 15910 (1999).
[16]H. Kawai, Y. K. Yeo, M. Saeys, and C. Joachim, Phys. Rev. B **81**, 195316 (2010).
[17]C. Joachim, D. Martrou, M. Rezeq, C. Troadec, D. Jie, N. Chandrasekhar, and S. Gauthier, J. Phys.: Condens. Matter **22**, 084025 (2010).
[18]M. Kepenekian, F. D. Novaes, R. Robles, S. Monturet, H. Kawai, C. Joachim, and N. Lorente, J. Phys.: Condens. Matter **25**, 025503 (2013).
[19]F. Ample, I. Duchemin, M. Hliwa, and C. Joachim, J. Phys.: Condens. Matter **23**, 125303 (2011).
[20]H. Kawai, F. Ample, Q. Wang, Y. K. Yeo, M. Saeys, and C. Joachim, J. Phys.: Condens. Matter **24**, 095011 (2012).
[21]R. Robles, M. Kepenekian, S. Monturet, C. Joachim, and N. Lorente, J. Phys.: Condens. Matter **24**, 445004 (2012).
[22]J. Y. Lee, J.-H. Cho, and Z. Zhang, Phys. Rev. B **80**, 155329 (2009).
[23]A. Kleshchonok, R. Gutierrez, and G. Cuniberti, Nanoscale **7**, 13967 (2015).
[24]E. Prati, M. Fanciulli, A. Calderoni, G. Ferrari, and M. Sampietro, J. Appl. Phys. **103**, 104502 (2008).
[25]D. Dovinos and D. Williams, Phys. Rev. B **72**, 085313 (2005).
[26]E. Prati, R. Latempa, and M. Fanciulli, Phys. Rev. B **80**, 165331 (2009).
[27]G. Platero and R. Aguado, Phys. Rep. **395**, 1 (2004).
[28]N. Ittah, G. Noy, I. Yutsis, and Y. Selzer, Nano Lett. **9**, 1615 (2009).
[29]S. Kohler, J. Lehmann, and P. Hänggi, Phys. Rep. **406**, 379 (2005).
[30]J. C. Cuevas and E. Scheer, *Molecular Electronics: An introduction to Theory and Experiment* (World Scientific, 2010).
[31]J. K. Viljas, F. Pauly, and J. C. Cuevas, Phys. Rev. B **77**, 155119 (2008).
[32]J. Deng, C. Troadec, H. K. Hui, and C. Joachim, J. Vac. Sci. Technol., B **28**, 484 (2010).
[33]P. K. Tien and J. P. Gordon, Phys. Rev. **129**, 647 (1963).
[34]A.-P. Jauho, N. S. Wingreen, and Y. Meir, Phys. Rev. B **50**, 5528 (1994).
[35]M. Moskalets and M. Büttiker, Phys. Rev. B **69**, 205316 (2004).
[36]J. K. Viljas, F. Pauly, and J. C. Cuevas, Phys. Rev. B **76**, 033403 (2007).
[37]D. Hirai, T. Hayakawa, S. Konabe, K. Watanabe, and T. Yamamoto, Jpn. J. Appl. Phys., Part 1 **48**, 08JB02 (2009).
[38]E. Rauls, J. Elsner, R. Gutierrez, and T. Frauenheim, Solid State Commun. **111**, 459 (1999).
[39]A. Pecchia, G. Penazzi, L. Salvucci, and A. Di Carlo, New J. Phys. **10**, 065022 (2008).
[40]J. VandeVondele, M. Krack, F. Mohamed, M. Parrinello, T. Chassaing, and J. Hutter, Comput. Phys. Commun. **167**, 103 (2005).
[41]J. P. Perdew, K. Burke, and M. Ernzerhof, Phys. Rev. Lett. **77**, 3865 (1996).
[42]M. L. Sancho, J. L. Sancho, J. L. Sancho, and J. Rubio, J. Phys. F: Met. Phys. **15**, 851 (1985).